High Resolution Nonreciprocal Microwave Interferometry of Moving Media and Structures

O. Gehre, H. M. Mayer, and M. Tutter

Max-Planck-Institut für Plasmaphysik, 8046 Garching, Germany

(Z. Naturforsch. **28 a**, 1443–1453 [1973]; received 1 June 1973)

Three experiments are described in which the relative motion of media or structures causes nonreciprocal effects of first order in v/c. The first two experiments deal respectively with the Fresnel effect due to the motion of a normal dielectric and the electron drift in the plasma of a glow discharge. The third experiment is a microwave analogon to the historical experiments of Harress, Pogany and Sagnac. To our knowledge these are the first investigations of the well-known effects under conditions where the transverse dimensions of the waves are comparable to the wave length. Under such conditions the nonreciprocal effects when expressed in fringe shifts (or phase angle) remain small. They could, however, be detected after the development of an elaborate microwave interferometry which could resolve fringe shifts down to the order of 10^{-6}.

I. Introduction

The determination of the state of relative motion of reflecting media is widely made by modern radar techniques which allow accurate measurements of the Doppler frequency shift of the reflected signal. On the other hand the state of relative motion of transparent media or even the state of rotation of a system in space can (at least in principle) be determined from the wavenumber shift of a transmitted signal. As early as in 1851 Fizeau [1] has shown that the phase velocity of a light ray could be influenced by the streaming of water through which it propagated (Figure 1 a). The result of this experiment

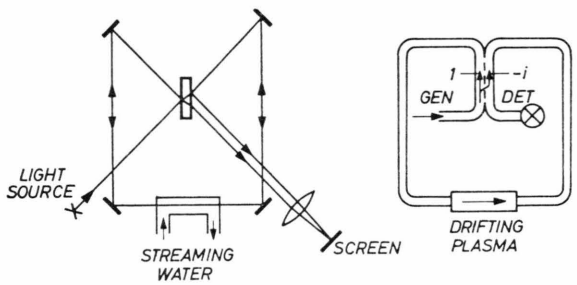

Fig. 1. a) Fizeau's experiment. b) Fizeau's experiment with guided waves.

is described by the well-known relation of Fresnel [2] and Lorentz [3] for the downstream increment of the phase velocity:

$$\Delta v_{\mathrm{ph}} = \boldsymbol{v}\left(1 - n^{-2} + \frac{\omega}{n}\frac{\mathrm{d}n}{\mathrm{d}\omega}\right) \tag{1}$$

Reprint requests to Frau Dr. L. Johannsen, Bibliothek, MPI für Plasmaphysik, *D-8046 Garching* bei München.

($n = k/k_0$ = refractive index for light of frequency ω, v = velocity of the medium $\ll c$). Equation (1) is equivalent to the relation

$$\Delta k = -\beta \cdot \frac{\omega}{c}\left(n^2 - 1 + \omega^2 \frac{\mathrm{d}n^2}{\mathrm{d}\omega^2}\right) = -\beta k_0 \left(\frac{\mathrm{d}k^2}{\mathrm{d}k_0{}^2} - 1\right) \tag{2}$$

($\beta = v/c$, $k_0 = \omega/c$) in terms of wavenumbers. The last equation corresponds to a fringe shift $\Delta N = \Delta k(L/\pi)$ between counterstreaming states of active length L. That a small phase shift $\Delta\Phi$ can generally be measured with much less accuracy than a frequency shift $\Delta\omega$ (which is equivalent to a monotoneously increasing phase, only limited by the time interval within which the measurement has to be completed) is certainly one of the reasons why methods based on the measurement of $\Delta\Phi$ have found much less practical application than those based on the measurement of $\Delta\omega$. However, modern ring laser techniques [4] have made it possible to convert a small nonreciprocal difference in optical distance into the beat frequency of two neighbouring, counterrotating modes. This possibility has improved very much the practical chances for methods based on nonreciprocal transmission. As an example we mention the experiments of Harress [5], Sagnac [6], Michelson and Gale [7], and Pogany [8] where two opposite light rays exhibit a nonreciprocal phase shift along a closed optical path in a rotating system (Fig. 2 a) which is given by $\Delta\Phi = k_0 \oint \boldsymbol{\beta}\,\mathrm{d}\boldsymbol{s}$ [Section V, Eq. (18)]. In a modern version of these experiments, using ring lasers, angular velocities of the order of one degree per minute have already been measured [4] and im-

provements of 2 orders of magnitude are still expected from present theory.

II. Nonreciprocal Microwave Interferometry

Figures 1 b and 2 b show the microwave versions of the above mentioned optical experiments in a schematic manner. We note that, (a) free propagation between optical components has been replaced by propagation through wave guides and that, (b) semitransparent mirrors have been replaced by 3 db couplers. Moreover, the phase shift for microwaves is about 5 orders of magnitude less than for optical frequencies. It follows, that an extremely sensitive interferometer must be used if the effect is to be detected at all.

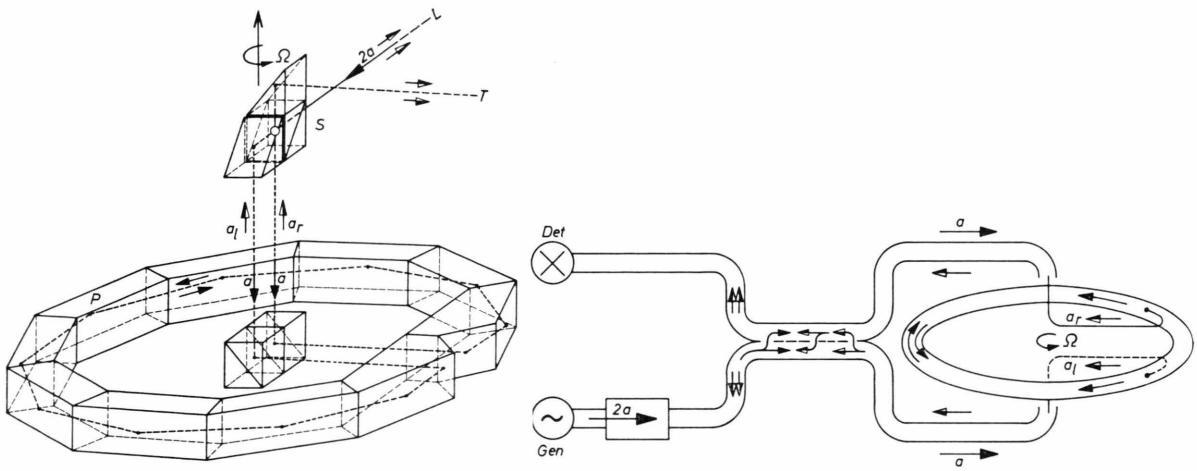

Fig. 2. a) The experiment of Harress and Pogany. The set of prisms P and the beam splitter S are rotating together while the light source L and the telescope T are stationary. (Observation is therefore made only during the short time intervalls when the beam is accepted by the telescope. This is, however, not harmful since the interference pattern is stationary although the intensity is fluctuaitng.) $2a$=incident intensity, $a_{r,1}$ intensities after clockwise or anticlockwise passage through the apparatus. b) A corresponding experiment with microwaves (schematic, intensities labeled as in Figure 2 a).

Another problem arises for microwaves which is absent for ray optics. Whereas rays which are reflected at the ends of the nonreciprocal section can easily be thrown out of the interferometer path by a slight inclination only of the confining surfaces, for the microwave interferometer no similar possibility exists. The only way to reduce the influence of these undesired reflections is good matching and means must be provided to control it.

The extreme sensitivity of the interferometer to matching conditions and/or unavoidable mechanical changes that go along with a reversal of the velocity $\boldsymbol{v}$ of the medium led to another innovation: The reversal of $\boldsymbol{v}$ was replaced by a reversal of the two oppositely directed wave trains. The latter is achieved by a two-way, two-channel waveguide switch which allows to interchange the connections of the interferometer section to generator and detector. The details of the microwave interferometer have already been described elsewhere [9]. We only mention briefly that the interferometer was equipped with two channels for the full display of the differential signal in the complex plane (amplitude and phase).

III. Shift of the Standing Wave in a Rotating, Dielectric Loaded Ring Cavity

Experimental arrangement

The object of this first experiment was to demonstrate the dragging of microwaves by a normal dielectric and rotation was chosen as the easiest way to move solid material at constant velocity in the laboratory. The arrangement used is shown schematically in Fig. 3 a whereas Fig. 4 gives the actual view of the device. The dielectric filling is removable and coupling is achieved by pins penetrating into a groove in the dielectric at positions A and B. The whole forms a "load" which is connected to the interferometer section of the apparatus outlined in Section II.

Circuit analysis

We assume field strength $\exp\{i\omega t\}$ at A. The transmitted field at $B(x)$ (Fig. 3 a) is then given by

$$E_{AB} = \exp\{i\omega t\}\{\tau_1 \exp\{-ik_1(L/2+x)\} \cdot \sum_{n=0}^{\infty} \exp\{-ik_1 nL\} + \tau_2 \exp\{-ik_2(L/2-x)\} \cdot \sum_{n=0}^{\infty} \exp\{-ik_2 nL\}\}. \quad (3)$$

Here $L = 2\pi R$ and $k_{1,2}$ are respectively the co-streaming and the counterstreaming wave vector components along the circular slot. $\tau_{1,2}$ are respectively (complex) transmission coefficients which take care of the coupling in either direction. Assuming the absence of any first order dependence of τ on velocity we take $\tau_1 = \tau_2 = \tau$ in the following. Setting

$$k_{1,2} = k_g \pm \Delta k, \quad (4)$$

we adjust k_g for resonance in the m-th circumferential mode in the absence of rotation:

$$k_g L \approx \mathrm{Re}\{k_g\} L = m \cdot 2\pi. \quad (5)$$

Denoting

$$\sigma = \exp\{L \cdot \mathrm{Im}\{k_g\}\}$$

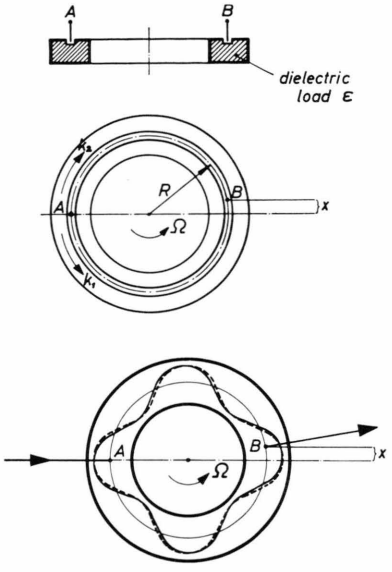

Fig. 3. a) Rotating slotted waveguide with dielectric load (schematic). b) Shift of the standing wave (schematic).

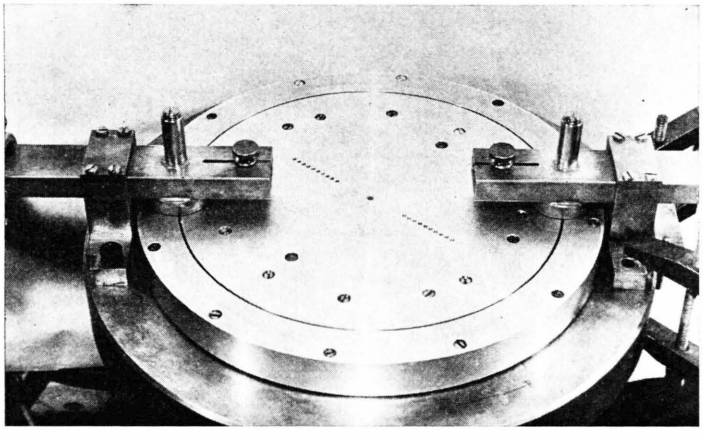

Fig. 4. Actual view of the device of Figure 3 a.

and assuming small damping (i.e. $1-\sigma \ll 1$) after a little algebra Eq. (3) can be written

$$E_{AB} = 2\tau\sigma^{1/2}(1-\sigma)^{-2}\exp\{i(\omega t - m\pi - \Delta k x)\} \cdot \{(1-\sigma)\cos k_g x - (1+\sigma)(\tfrac{1}{2}\Delta k L)\sin k_g x\} \quad (6)$$

where only terms up to first order in $\Delta k \cdot L$ have been retained. Exchange of generator and detector – which is equivalent to a replacement of x by $-x$ – transforms Eq. (6) into

$$E_{BA} = 2\tau\sigma^{1/2}(1-\sigma)^{-2}\exp\{i(\omega t - m\pi + \Delta k x)\} \cdot \{(1-\sigma)\cos k_g x - (1+\sigma)(\tfrac{1}{2}\Delta k L)\sin k_g x\}. \quad (7)$$

From Eqs. (6) and (7) we derive the quantity

$$2\frac{E_{AB}-E_{BA}}{E_{AB}+E_{BA}} = -2\frac{\Delta k L}{1-\sigma}\,\mathrm{tg}\,k_g x \quad (8)$$

which is a measure of the nonreciprocity of the four terminal AB.

The denominator $1-\sigma$ on the right-hand side of Eq. (8) plays the role of an enhancement factor. It can be understood qualitatively by observing that the standing wave (Fig. 3 b) is the result of a superposition of many turns of the same wave upon itself, each turn proceeding in phase by $\Delta k \cdot L$ and decreasing, but slightly, in amplitude. Since the net effect on the integrated pattern is accumulative, it should be proportional to the number of turns that

can contribute, which is $(1-\sigma)^{-1}$. The value of this denominator can be determined experimentally from the resonance width $\Delta\omega$ of the ring cavity at rest. After the summation in Eq. (3) is carried out we find (setting $\tau_1=\tau_2=\tau$, $k_1=k_2=k_g$)

$$|E_{AB}|^2=\frac{4\tau^2\sigma\cos^2(k_g x)}{|1-\sigma\exp(i k_g L)|^2}\,. \tag{9}$$

Since $\sigma\approx 1$ and $|x|\ll L$, it is the denominator which determines the shape of the resonance centered at $k_g L=2\pi$ m. The increase in phase angle $\Delta k_g L$ which is necessary to double its resonance value $(1-\sigma)^2$ is simply given by

$$1-\sigma=L\Delta k_g=L\frac{\mathrm{d}k_g}{\mathrm{d}\omega}\frac{\Delta\omega}{2}=m\pi\frac{\Delta\omega}{\omega}\frac{\omega}{k_g}\frac{\mathrm{d}k_g}{\mathrm{d}\omega} \tag{10}$$
$$=\frac{m\pi}{Q}\frac{\omega}{k_g}\frac{\mathrm{d}k_g}{\mathrm{d}\omega}$$

where a "Q value" has been defined by $Q^{-1}=\Delta\omega/\omega$.

With the help of the last equation, Eq. (8) can be written in the form

$$\frac{E_{AB}-E_{BA}}{E_{AB}+E_{BA}}=-\Delta k\,L\,\mathrm{tg}(k_g x)\frac{Q}{m\pi}\frac{k_g}{\omega}\frac{\mathrm{d}\omega}{\mathrm{d}k_g}\,. \tag{11}$$

Following v. Laue [10] we feel entitled to replace circular by rectilinear motion. Setting $k=k_g$ in Eq. (2) we find

$$\Delta k=-\beta k_0(\mathrm{d}k_g^2/\mathrm{d}k_0^2-1)\,. \tag{12}$$

Combining Eqs. (12), (11) and (5) and introducing at the same time the dispersion of a waveguide that is loaded with a dielectric, i. e.

$$\varepsilon k_0^2=k_g^2+k_c^2$$

we obtain

$$\frac{E_{AB}-E_{BA}}{E_{AB}+E_{BA}}=2\beta\frac{k_g}{k_0}Q(1-\varepsilon^{-1})\,\mathrm{tg}(k_g x)\,. \tag{13}$$

(The dielectric used was Polystyrol and the neglect of dispersion and loses in Eq. (13) is well justified. Defining $\varepsilon_{\mathrm{eff}}$ from the dispersion of the corresponding rectilinear waveguide, i. e. $\varepsilon_{\mathrm{eff}}k_0^2=k_g^2+k_c^2$, values of $\varepsilon_{\mathrm{eff}}$ between 1.9 and 2.06 have been obtained whereas from the literature $\varepsilon\approx 2.5$. The discrepancy is attributed to i) the presence of the groove for the pick-up probe, ii) curvature and possibly iii) individual deviations of the sample. Equation (13) reflects the shift of the standing wave — as obtained from Eq. (6) — by the distance

$$\Delta x=-\frac{\Delta k}{k_g}\cdot\frac{1+\sigma}{1-\sigma}\cdot\frac{L}{2}\approx 2\frac{\beta}{k_0}Q(1-\varepsilon^{-1}) \tag{14}$$

due to rotation.

Experimental results

The signal at the receiver probe is enhanced for $0<x<\lambda_g/4$. The nonreciprocity as defined by the left-hand side of Eq. (8) tends towards infinity as $k_g\cdot x$ approaches $\pi/2$. However, at the same time the transmitted power tends to zero and the signal will be lost in noise. For most measurements we therefore used $|k_g\cdot x|\approx\pi/4$ as a compromise. Figure 5 shows experimental results for $\lambda_0=3.29$ cm, $\lambda_g=2.65$ cm, $Q=830$, $D=2R=17.75$ cm. Typically at 150 revolutions per second the shift of the standing wave was $\Delta x=1.25\,\mu$.

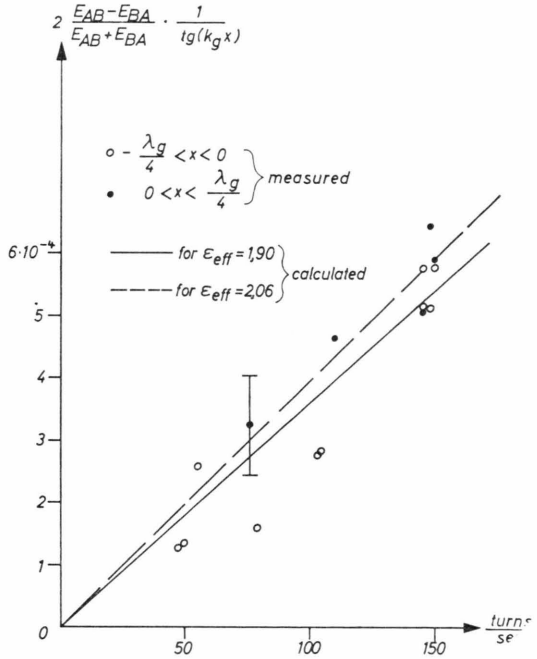

Fig. 5. Nonreciprocal transmission of the rotating slotted waveguide with dielectric load.

IV. Dragging by Electron Drift in a Glow-discharge

In this second experiment we take advantage of the high speed at which the refractive "electron fluid" in a glow discharge drifts from the cathode towards the anode. However, the advantage of the easily obtainable high speeds is to a great deal compensated by the particular form of the "cold" plasma dielectric constant which under neglect of collisions is given by

$$\varepsilon=n^2=1-\omega_p^2/\omega^2\,. \tag{14}$$

(ω_p = electron plasma frequency).

It is easily verified that the bracket of Eq. (2) vanishes if n is given by Eq. (14), in other words: there is no dragging in a uniform cold plasma [11]. This property is a consequence of the assumption used in the derivation of Equation (14). It is the assumption of noninteracting particles, which are forced to oscillate under the influence of a transverse wave and don't have the possibility to store and release potential energy during one cycle of oscillation.

The "laminated dielectric" model

In reality the dielectric represented by a glow discharge is neither cold nor uniform nor free from collisions. For frequencies $\omega \gtrsim 2\,\omega_p$ we may assume that electrostatic waves are sufficiently suppressed by Landau damping. If at the same time $\nu_{coll} \ll \omega$ we may also disregard collisions. The density profile of a glow discharge at low pressures is flat on the axis and has a steep drop in the sheath region. A similar profile is expected for the drift velocity v_d of the electrons. For simplicity we assume the permittivity-velocity profile

$$\begin{aligned} &0<r<a: \quad \varepsilon=\varepsilon_1=1-\omega_p^2/\omega^2, \quad v_d=v \\ &a<r<b: \quad \varepsilon=\varepsilon_2, \qquad\qquad\quad v_d=0 \end{aligned} \tag{15}$$

where a and b are respectively the inner radii of the discharge tube and its metallic enclosure whereas ω_p and v represent suitable average values of $\omega_p(r)$ and $v_d(r)$ for $r \leqq a$.

The principal novelty of this experiment with respect to the preceeding one is the existence of a differential velocity in the dielectric load of the waveguide. In previous papers [12, 13], we have derived expressions for Δk for the profile given by Eq. (15) in the limit $(b-a)/a \ll 1$:

$$\Delta k = -\beta k_0 \frac{b-a}{b} \frac{1}{\varepsilon_2}\left(\varepsilon_2 - 1 + \frac{\omega_p^2}{\omega^2}\right) \cdot \frac{\omega_p^2}{\omega^2} \quad (\mathrm{TE}_{11}\text{-mode}), \tag{16 a}$$

$$\Delta k = -\beta k_0 \frac{b-a}{b} \frac{2}{\varepsilon_2}\left(\frac{2.4^2}{b^2 k_0^2} + \varepsilon_2 - 1 + \frac{\omega_p^2}{\omega^2}\right) \cdot \frac{\omega_p^2}{\omega^2} \quad (\mathrm{TM}_{01}\text{-mode}), \tag{16 b}$$

$$\Delta k = 0 \qquad (\mathrm{TE}_{01}\text{-mode}). \tag{16 c}$$

In this experiment we had always

$$\langle \omega_p^2/\omega^2 \rangle_{av} \ll 1 < \varepsilon_2 - 1 \approx 3.6\,. \tag{17}$$

Excessive noise rendered the measurement unreliable whenever $\omega_p^2 \ll \omega^2$ was violated. Thus, for our purpose, we can neglect the ω_p^4/ω^4 terms in Eqs. (16 a, b) which makes Δk proportional to the discharge current $I = e\langle n v\rangle \pi a^2$. (The product $\beta\,\omega_p^2$ of the model quantities is identified with an average value $\langle \beta\,\omega_p^2\rangle$ for the actual discharge.) Inserting now the relation $(\omega_p/(2\pi \cdot 10^{10}\,\mathrm{Hz}))^2 = 0.8\,n/(10^{12}\,\mathrm{cm}^{-3})$ into Eqs. (16 a, b) we find for the phase increments $\Delta k \cdot L$ (L = length of the interferometer path coinciding with that of the discharge):

$$-\Delta k \cdot L\ (\text{degrees}) = 2.12 \cdot 10^{-3} \frac{\varepsilon_2 - 1}{\varepsilon_2} \frac{b-a}{b} \cdot \frac{L\lambda_0}{a^2} \cdot I\ (\text{amps.}) \quad (\mathrm{TE}_{11}\text{-mode}) \tag{17 a}$$

$$-\Delta k \cdot L\ (\text{degrees}) = 4.2 \cdot 10^{-3} \frac{1}{\varepsilon_2} \cdot \left[\left(\frac{0.38\,\lambda_0}{b}\right)^2 + \varepsilon_2 - 1\right] \frac{b-a}{b} \cdot \frac{L\lambda_0}{a^2} \cdot I \quad (\mathrm{TM}_{01}\text{-mode}) \tag{17 b}$$

where $\lambda_0 = 2\pi/k_0$.

Geometry

In earlier arrangements [14, 15] a U-shaped discharge had been introduced through vertical "chimneys" into a straight waveguide section. Apparently, mode transformations and time varying matching conditions rendered the measurements very erratic under conditions where more than one mode could propagate. The arrangement of Fig. 6 allowed a better match to dipolar symmetry and avoided the occurrence of high density plasma within the interferometer path. At the same time the diameter of the waveguide was reduced to exclude all but the TE_{11}-like mode from propagation.

Discharge

The discharge was a low pressure (typically 3×10^{-3} torr of Argon) glow discharge. (The oxyde coated thyratron cathodes were kindly provided from the Philips Company Eindhoven.) The average electron density in the active part of the column was determined by microwave techniques. Detuning of a resonant cavity at 1.86 GHz and propagation of 3.3 cm waves along the column yielded values which are typically represented by $\langle \mathrm{fp}/10^{10}\,\mathrm{Hz}\rangle = 0.046\,I/A$ or $\langle n_e\rangle/\mathrm{cm}^{-3} \approx 5.8 \times 10^{10}\,I/A$ and $v_d \approx 5 \times 10^7$ cm/sec.

Results

TE_{11} mode: The results with the arrangement of Fig. 6 are plotted in Figure 7. Inserting experimental parameters $a = 0.805$ cm, $(\varepsilon_2 - 1)(b-a)/\varepsilon_2 b = 0.125$ into Eq. (17 a) we find for the average wavelength $\lambda_0 = 3.37$ cm of Fig. 7 $-\Delta k\, L/I = 0{,}069$ degrees/amp. Although the accuracy of the measurements did not allow to distinguish between the different wavelengths of Fig. 7, the overall agreement between the measurements and the predictions of the model are quite satisfactory. The measurements have revealed that for small electron densities the presence of the glass tube becomes more important than the presence

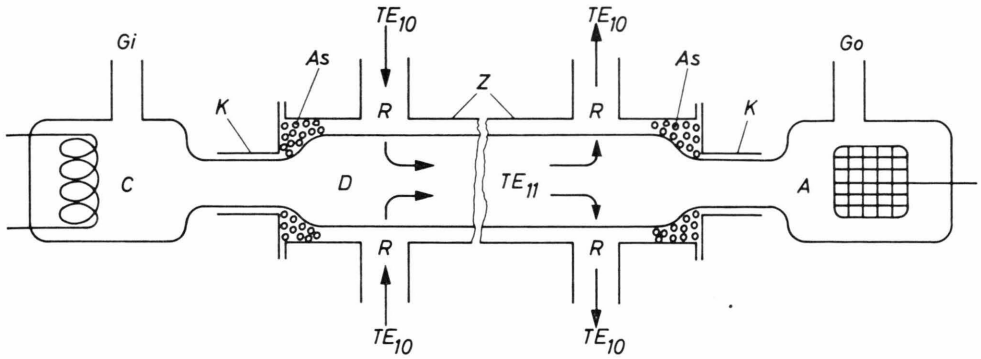

Fig. 6. A glow discharge as a moivng dielectric load. C cathode, G_i gas inlet, G_0 pump lead, A anode, Z circular waveguide, R rectangular waveguides, D discharge tube, As microwave absorber, K end tubes (below cut-off).

of an ion sheath. They therefore stimulated the extension of a model of two dielectric layers moving with a common velocity [12] to a model of many layers moving with parallel velocities of individual magnitude [13].

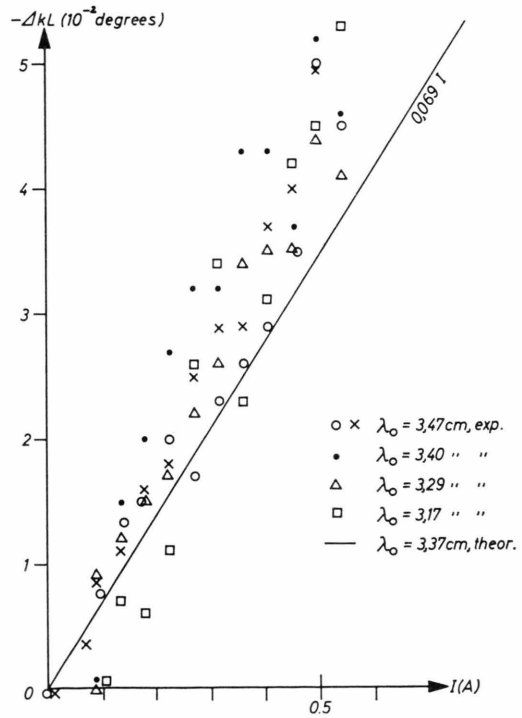

Fig. 7. Nonreciprocal transmission due to electron drift.

TM_{01} and TE_{01} modes: Measurements have been carried out in the U-shaped discharge geometry [14, 15] and appeared to be more affected by noise and uncontrolled distortions than the measurements for the TE_{11}-like mode mentioned above. Nevertheless the trend of these measurements seemed to agree with Eqs. (16 b, c) which predict more than twice the dragging for the TM_{01}-mode and no dragging for the TE_{01}-mode.

V. Rotating Annular Cavity

When the dielectric load is removed in the arrangement of Fig. 3 a an empty cavity is left back which, however, at the same time has lost its sensitivity to rotation. Indeed, the motion of the cavity walls will produce only a negligible effect [13]. If, however, we change over to the coupling system of Fig. 8 the waves on their way from generator to detector, follow loops with a definite sense (Figure 2 b). This sense may be either parallel or opposed to the sense of the mechanical rotation and nonreciprocal propagation can indeed be observed.

Optical experiments

The first optical experiment has been carried out by Harress in the laboratory [5] and dates back as far

as 1911. It was followed by similar experiments in the laboratory [6] and on a large scale by Sagnac and by Michelson and Gale [7]. The following simple argument can explain the experiments in which opposite light rays in air are conducted on closed paths by means of mirrors.

For simplicity suppose that a large number of mirrors makes the deviation from a circular path negligible. The time for the ray to go round is then approximately given by $\Delta t = L/c$ where $L = 2\pi R$. During this time, however, the mirror from which it started has moved on by an additional distance $v \cdot \Delta t$ along the circumference. Neglecting higher order terms in v/c, this will also be the incremental distance which the ray needs to catch up with the original mirror. In terms of phase angle this amounts to

$$\Delta\Phi = k\, v\, \Delta t = (v/c)\, k\, L \tag{18}$$

or

$$\Delta\Phi/2\pi = \Delta N = \beta (p_0 R/\hbar)$$

with

$$p_0 = \hbar\, \omega/c = \hbar\, |\boldsymbol{k}| \tag{19}$$

where the sign reverses with the sign of $\boldsymbol{k}$. The last equation shows the intimate relationship between the observed fringe shift ΔN and the orbital angular momentum of a photon as obtained from the De Broglie relationship.

Analogy to the Aharanov-Bohm experiment

At this point we want to mention an analogy to the experiment suggested by Bohm and Aharanov [16]. In this experiment two electron beams are separated from a common original one by two narrow slits in a diaphragm and their interference is observed on a screen. Along their path a vector potential $\boldsymbol{A}$ exists which is oriented perpendicular to the slits whereas the magnetic induction $\boldsymbol{B} = \nabla \times \boldsymbol{A}$ across all possible paths of electron flight is negligable. The fringe shift is given by [16]

$$\Delta N = \frac{\Delta\Phi}{2\pi} = \frac{1}{h}\frac{9}{c}\int^{\text{c.o.}} \boldsymbol{A}\, \mathrm{d}\boldsymbol{s} \tag{20}$$

(q is the electron charge and $\mathrm{d}s$ is the path element) where we integrate around the closed orbit obtained by reversal of one of the electron paths. The above integral is the action integral of the canonical momentum

$$\boldsymbol{\pi} = \boldsymbol{p} + (q/c)\, \boldsymbol{A}$$

where only the second term yields a net contribution around the closed orbit.

The analogy between the two experiments becomes evident when Eq. (18) is written in the form

$$\Delta N = (1/2\,h)\left\{\int^{\text{c.c.w.}} \boldsymbol{p}^{+}\, \mathrm{d}\boldsymbol{s} - \int^{\text{c.w.}} \boldsymbol{p}^{-}\, \mathrm{d}\boldsymbol{s}\right\}$$

with c.c.w. and c.w. closed orbits and

$$p^{\pm} + \hbar\,(\omega^{\pm}/c) = (\hbar/c)\,(\omega \pm v\, k)$$

where the minus sign occurs in front of the second integral because the sense of integration has been reversed and the factor $1/2$ is due to the replacement of half orbits by full orbits. The above action integrals can be related to the "orbital (canonical) angular momenta" according to the scheme

$$(1/2\,\pi)\int^{\text{c.c.w.}} \boldsymbol{p}\, \mathrm{d}\boldsymbol{s} = (1/2\,\pi)\int^{\text{c.c.w.}} p_\varphi\, \mathrm{d}s_\varphi = \int^{\text{c.c.w.}} [\boldsymbol{r} \times \boldsymbol{p}]\, \mathrm{d}\boldsymbol{\alpha}/2\,\pi\,.$$

(The integral $\int^{\text{c.c.w.}} p_r\, \mathrm{d}s_r$ can be seen to vanish in a conservative force field.) In both experiments ΔN is a direct measure of the canonical angular momentum of the closed orbit in units of $\hbar$.

Waveguide modes

The argument leading to Eq. (18) breaks down for propagation in refractive material like glass as in the experiment of Harress. The following analysis includes refraction and dispersion and is also applicable to waveguide modes. We describe the propagation in a dielectric loaded annular cavity which is fed from the axis through a rotating "spoke" (Fig. 8) by means of directional couplers. As long as there is no dielectric load the rotation of the cavity alone (the walls of which we assume to have infinite conductivity) remains immaterial and any effect has therefore to be attributed to the rotation of the spoke.

Description in rectilinear tangential frames

Based on the arguments quoted in Section III we first give a description in tangential rectilinear frames. We assume that the couplers, while in motion, are still carrying their feeding frequency $\omega_1 = c\,\varkappa_0$ (Fig. 9) which they had on the axis of rotation. This assumption should be justified if i) the feeding mode on the axis has rotational symmetry ($m = 0$ mode) and ii) if higher order terms in β can be neglected (see below). We proceed in two steps. In the first step we launch a wave from the moving coupler into a ring which is fixed (i. e.

by its dielectric load) in the laboratory. In the coupler the fields will contain a spatial spectrum of $\varkappa$-vectors. However, only one mode will propagate before being absorbed by the absorber As. Let the wave vectors for the mode propagating in the preferred direction be

$$\underset{\text{in the coupler}}{(\varkappa_0 = \omega_1/c, \varkappa_x, \varkappa_y)} \quad \text{and} \quad \underset{\text{in the laboratory}}{(k_0 = \omega_2/c, k_x, k_y)}.$$

Out of the six components only $\varkappa_0$ and k_y are considered to be known a priori. The rest of the components are determined by the conditions i) that the launched wave has to obey the dispersion relation in the annular waveguide which we write

$$k_x = k_x(k_0, k_y) \tag{21}$$

ii) that the wave vector has to transform – within first order accuracy in β – from one system to the other, i. e.

$$k_0 = \varkappa_0 + \beta \varkappa_x, \tag{22}$$

$$k_x = \varkappa_x + \beta \varkappa_0 \tag{23}$$

(Equations (22) and (23) are the Lorentz transformations for wavenumber and frequency in the limit $\beta \ll 1$).

To these three equations we could add the dispersion $\varkappa_x = \varkappa_x(\varkappa_0, \varkappa_y)$ for the compler, but, as long as we are not interested in $\varkappa_y$ we are satisfied with a system of three equations for the three unknowns k_0, k_x, $\varkappa_x$.

For $\beta = 0$ we assume that – by proper choice of dimensions – this system has the solution

$$k_{00} = \varkappa_0;\ k_{x0} = k_x(\varkappa_0, k_y);\ \varkappa_{x0} = k_{x0}. \tag{24}$$

Keeping $\varkappa_0$ fixed for $0 < \beta \ll 1$, this solution will be slightly modified by small increments which we give in differential form. We then have the three following equations

$$\Delta k_0 = \beta \varkappa_x, \tag{22 a}$$

$$\Delta k_x = \Delta \varkappa_x + \beta \varkappa_0, \tag{23 a}$$

$$\Delta k_x = (\mathrm{d}k_x/\mathrm{d}k_0)\,\Delta k_0 \tag{21 a}$$

for the three unknown increments Δk_0, Δk_x, $\Delta \varkappa_x$. Their combination yields within first order terms

$$\Delta k_x = (\Delta k_x)_{\text{coupler}} = \beta \varkappa_x \frac{\mathrm{d}k_x}{\mathrm{d}k_0} \approx \beta k_x \frac{\mathrm{d}k_x}{\mathrm{d}k_0} = \frac{\mathrm{d}k_x^2}{\mathrm{d}k_0^2} \cdot \beta k_0. \tag{25}$$

In the second step we accelerate the dielectric load to the velocity of the coupler. The resulting dragging by the dielectric has been investigated in the first experiment and was given by Eq. (2)

$$(\Delta k_x)_{\text{drag}} = -\,(\mathrm{d}k_x^2/\mathrm{d}k_0^2 - 1)\,\beta k_0. \tag{2 a}$$

Combining the last two equations we find

$$(\Delta k_x)_{\text{rot}} = (\Delta k_x)_{\text{coupler}} + (\Delta k_x)_{\text{drag}} = \beta k_0. \tag{26}$$

We reproduced the result of our simple argument, however, this time showing that it should not depend on the transverse geometry of the waveguide nor on its dielectric load. (Similar arguments have already been used by Einstein [17] and later by v. Laue [18] to explain the experiment of Harress [5].) Aside of Eq. (26) we may write down

$$(\Delta k_0)_{\text{rot}} = (\Delta k_0)_{\text{coupler}} = \beta k_x \tag{27}$$

which follows from Eqs. (22 a) and (23 a) within first order terms. Finally Eqs. (26) and (27) can be written in the form

$$(k_0)_{\text{rot}} = (k_0)_{\text{nonrot}} + \beta \mathbf{k_x},$$

$$(k_x)_{\text{rot}} = (k_x)_{\text{nonrot}} + \beta k_0 \tag{28}$$

which we have earlier [13] called a transmodification because it does not really describe the difference in view of two observers moving at constant velocity relative to each other but rather the modification of a dispersion law due to relative motion of matter (and/or energy). In order to deduce a one-to-one correspondence from a transmodification we need one more condition. In our case where we compare modes of the same feeding frequency on the axis of rotation this condition is $\Delta \varkappa_0 = 0$.

Description in cylindrical frames

The above result must also be describable in rotating cylindrical frames. To do this we need a transformation which – within first order β terms – carries over scalings from the lab to the rotating frame. The transformation is easily obtained for the cylindrical "wavevector" $(k_0 = \omega/c,\ k_r,\ m/r)$ describing a cylindrical mode $J_m(r k_r)\ \exp\{i(m\varphi - \omega t)\}$ whose components for large m are related to the components in the tangential rectilinear system by

$$k_r \to k_y;\quad m/r \to -k_x. \tag{29}$$

If the primed frame rotates with an angular velocity $\Omega = (0, 0, \Omega)$ in the unprimed frame we find immediately

$$\beta \to -\Omega r/c \tag{30}$$

and

$$\omega' = \omega - \Omega m,\quad k_r' = k_r,\quad m' = m. \tag{31}$$

The first of these equations becomes evident when accepting the role of a rotating observer who watches a mode in the laboratory. The third equation fol-

lows from the topological quality of m being the number of azimuthal periods. The other equation is trivial. Unlike Eqs. (28), Eqs. (31) are geometrical transformations based on simultaneity which do not correctly describe physical events. We may, however, use them to translate the physical event described by Eqs. (28) into the notation of rotating cylindrical frames if, by means of the transitions (29) and (30) we introduce them into the right-hand side of Equations (31). For m and ω we obtain

$$(\omega)'_{\mathrm{rot}} = (\omega)_{\mathrm{rot}} - \Omega m = (\omega)_{\mathrm{nonrot}} - \Omega r(-m/r) - \Omega m = (\omega)_{\mathrm{nonrot}} \tag{32}$$

$$(m)'_{\mathrm{rot}} = (m)_{\mathrm{rot}} = (m)_{\mathrm{nonrot}} + \Omega r^2 \omega/c^2 . \tag{33}$$

Equations (32), (33) express the transmodification in the rotating cylindrical frame. We have not derived these equations in the rotating frame. This is not trivial because the constitutional equations relating $\boldsymbol{E}$ and $\boldsymbol{B}$ with $\boldsymbol{D}$ and $\boldsymbol{H}$ are changed in this frame. Heer [19] has given an analysis on the grounds of general relativity, obtaining results which agree with the above ones for the first order effects. A direct interpretation of Eqs. (32) and (33) may, however, be obtained in the quantum picture. We first assume a particle of mass M and velocity v_M moving radially outward between $r=0$ and $r=R$. In the rotating system the particle "feels" rotation only through the presence of an effective force

$$\boldsymbol{F}_{\mathrm{eff}} = -M[2\,\boldsymbol{\Omega}\times\boldsymbol{v}_M + \boldsymbol{\Omega}\times(\boldsymbol{\Omega}\times\boldsymbol{r})] = \boldsymbol{F}_{\mathrm{cor}} + \boldsymbol{F}_{\mathrm{cen}} . \tag{34}$$

The second term (centrifugal force) is directed radially and increases the kinetic energy of the particle. The first term (Coriolis force) acts perpendicular on the particle's velocity and deviates it from a straight line to a curve of "free fall to the side". Replacing the particle by a quantum we have to make the substitutions

$$M \to \hbar\,\omega/c^2 \tag{35}$$

and

$$\boldsymbol{v}_{\mathrm{M}} \to \boldsymbol{v}_{\mathrm{Q}} \tag{36}$$

where $\boldsymbol{v}_{\mathrm{Q}}$ is the velocity at which the energy of the quantum propagates. The latter is usually identified with the group velocity of the wave. Neglecting terms of higher than first order in the velocity we can drop the centrifugal force, thereby keeping the energy constant. This immediately confirms Equation (32). On the other hand the incremental angular momentum which the quantum acquires from the action of the Coriolis force during its radial flight will be

$$(\Delta J)_{\mathrm{cor}} = (\Delta m)_{\mathrm{cor}}\cdot\hbar = -\Delta k_x R\hbar = \int_{t_0}^{t_R} (\boldsymbol{r}\times\boldsymbol{F}_{\mathrm{cor}})_z\,\mathrm{d}t = \int_0^R r(F_{\mathrm{cor}})_\varphi \frac{\mathrm{d}r}{v_{\mathrm{Q}}} = -2\frac{\hbar\,\omega}{c^2} \int_0^R r\,\Omega\cdot v_{\mathrm{Q}}\frac{\mathrm{d}r}{v_{\mathrm{Q}}} = -\frac{\hbar\,\omega}{c^2} R^2\,\Omega \tag{37}$$

where the velocity v_{Q} has dropped out. The result agrees with Eq. (33) if we assume that the action of the Coriolis force has to be compensated by a difference $(m)_{\mathrm{rot}} - (m)_{\mathrm{non\,rot}}$ of opposite sign.

Enhancement by multiple loops

As in the first experiment, the effect is enhanced by multiple cycling of the wave through the ring resonator. The transmitted field is calculated as in Eqs. (3) to (8) under the slight modification that x is set equal to zero and that the series starts with a full turn instead of a halfturn. Instead of Eq. (3) we then have

$$\boldsymbol{E}_{\mathrm{AB}} = \exp\{i\,\omega\,t\}\,\tau\sum_{j=1}^{\infty}\exp\{-i\,k_1\,j\,L\} = \exp\{i\,\omega\,t\}\,\tau\frac{\sigma\exp\{-i\,\Delta k\,L\}}{1-\sigma\exp\{-i\,\Delta k\,L\}} \tag{39}$$

where we again have assumed that the cavity was tuned to resonance [Equation (5)]. Reversing A and B simultaneously with the sign of Δk we calculate for the transmitted signals the ratio

$$2\frac{E_{\mathrm{AB}}-E_{\mathrm{BA}}}{E_{\mathrm{AB}}+E_{\mathrm{BA}}} = \frac{\exp\{-i\,\Delta k\,L - \exp\{+i\,\Delta k\,L\}}{1-\sigma} \simeq \frac{-2\,i}{1-\sigma}\Delta k\,L .$$

Introducing $\Delta k = (k_x)_{\mathrm{rot}} - (k_x)_{\mathrm{non\,rot}} = \beta\,k_0$ from Eq. (28) and

$$(1-\sigma)^{-1} = \frac{Q}{\pi\,m}\frac{k_g^2}{\omega^2}\frac{\mathrm{d}\omega^2}{\mathrm{d}k_g^2}$$

from Eq. (10) we finally have

$$2(E_{\mathrm{AB}}-E_{\mathrm{BA}})/(E_{\mathrm{AB}}+E_{\mathrm{BA}}) = -i\,4\,\beta\,Q\,k_g/k_0 . \tag{40}$$

The factor i means that the phase rather than the amplitude of the transmission is nonreciprocal.

Apparatus

The working principle of the apparatus had already been demonstrated in Fig. 2 b, whereas details

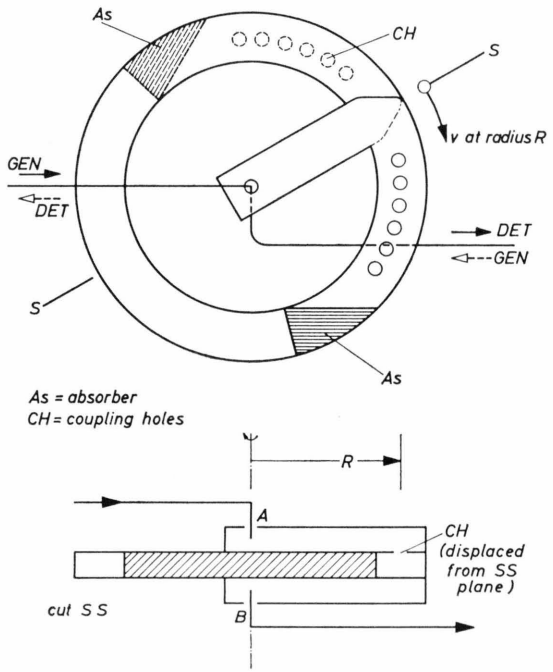

Fig. 8. Rotating ring cavity with directional couplers (schematic).

Tab. 1

λ_0 [cm]	λ_g [cm]	Q	$(c/Q)\cdot k_0/k_g$ [cm/sec]
3.67	6.14	1240	4.03×10^7
3.38	5.01	1480	2.99×10^7
2.99	3.95	1860	2.13×10^7

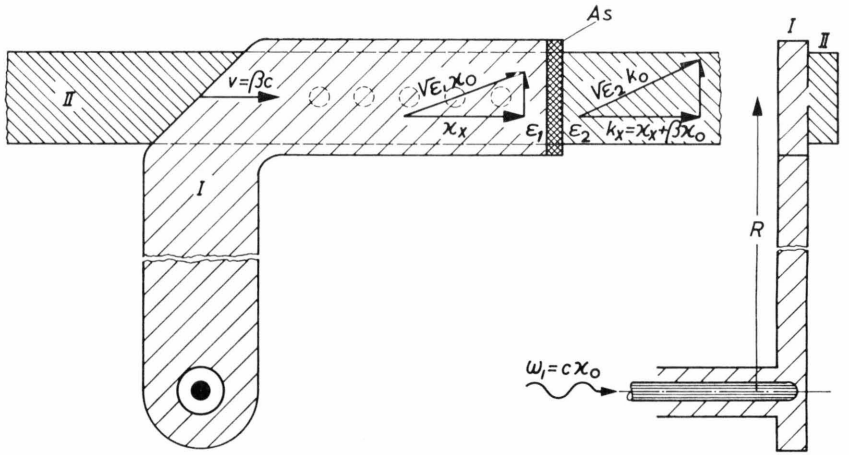

Fig. 9. Feeding mechanism of the rotating ring cavity.

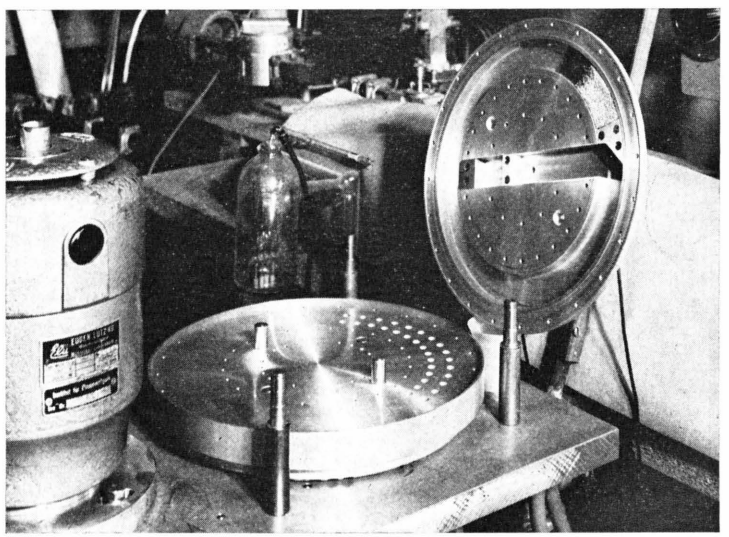

Fig. 10. Actual view of the rotating ring cavity with top coupler.

of the feeding mechanism have been schematically depicted in Figures 8 and 9. As in the preceeding experiments the nonreciprocal section A B is not directly connected to generator and detector (as indicated in these figures) but is inserted instead into the path of the high resolution microwave interferometer mentioned in Section II (i. e. between terminals ST_1 and ST_2 of Ref. [9]). The actual view of the rotating part is given in Figure 10. The ring cavity is covered by a disc with a double row of coupling holes. The lid (standing upright in Fig. 10) contains the coupler consisting of a radial and an annular section the last portion of which is filled by absorbing material.

Experimental results

Figure 11 shows the nonreciprocal transmission obtained with a cavity of $R = 8.8$ cm at the three different frequencies listed in the table below. The straight line is predicted from Eq. (40) and agreement between measurement and theory is within the expected experimental error.

VI. Conclusions

Nonreciprocity of first order in v/c in the transmission of guided microwaves through moving media and rotating structures has been demonstrated. In the case of an electron plasma which drifts along the axis of a circular waveguide agreement could be obtained with a dielectric model [13] that extends the wellknown Fresnel-Lorentz formula to propagation in laminated guiding structures with nonuniform velocities. The detection of phase shifts $\Delta\Phi/2\pi$ of the order 10^{-6} has been achieved by a noise reducing interferometry [9] which could be applied to other nonreciprocal phenomena in the waveguide range.

Acknowledgements

The authors wish to thank Mr. J. Prechtl for building most of the non-commercial parts of the apparatus and for his assistance in the measurements. The help of Messrs. F. Brandl, T. Kaltner, H. Rebischki and of Miss C. Wallner is also greatfully acknowledged.

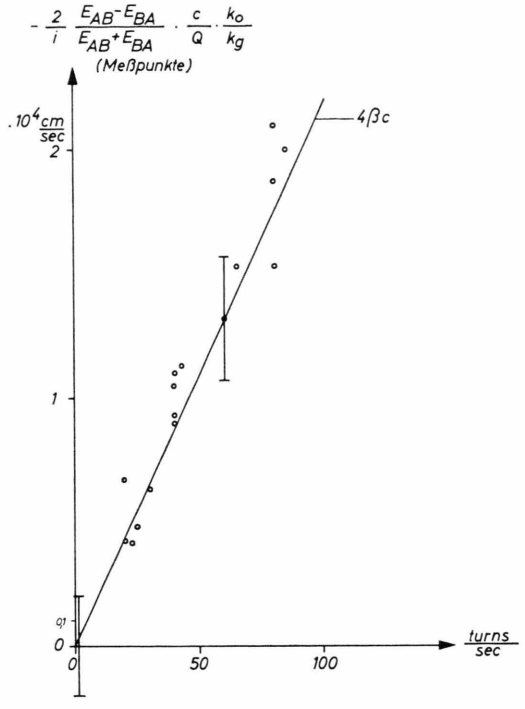

Fig. 11. Nonreciprocal transmission of the rotating ring cavity.

[1] H. Fizeau, C. R. Acad. Sci. Paris **33**, 349 [1851].
[2] F. Fresnel, Ann, Chim. Phys. **9**, 47 [1818].
[3] H. A. Lorentz, Versuch einer Theorie der elektrischen und optischen Erscheinungen in bewegten Körpern, Leiden 1895.
[4] For a survey article see: F. Malota, Laser und angewandte Strahlentechnik **2**, 13 [1970].
[5] F. Harress, Thesis, Jena 1911, see Ref. [8].
[6] G. Sagnac, C. R. Acad. Sci. Paris **157**, 708 and 1410 [1913]; J. de Phys. (5) **4**, 177 [1914].
[7] A. M. Michelson and H. G. Gale, Astrophys. J. **61**, 140 [1925].
[8] B. Pogany, Ann. Physik. Lpz. **80**, 217 [1926]; **85**, 244 [1928].
[9] O. Gehre, H. M. Mayer, and M. Tutter, IEEE, **IM-18**, 194 [1969].
[10] M. v. Laue, Ann. Physik Lpz. **62**, 448 [1920].
[11] E. Räuchle, Plasma Physics (J. of Nucl. En., Part C) **5**, 329 [1963].
[12] O. Gehre, H. M. Mayer, and M. Tutter, Z. Naturforsch. **27 a**, 215 [1972].
[13] O. Gehre, H. M. Mayer, and M. Tutter, Z. Naturforsch. **28 a**, 885 [1973].
[14] O. Gehre, H. M. Mayer, and M. Tutter, Phys. Letters **28A**, 35 [1968].
[15] O. Gehre, H. M. Mayer, and M. Tutter, IPP Report 3/94, Garching 1969.
[16] see: The Feynman Lectures by R. P. Feynman, R. B. Leighton, and M. Sands, Addison-Wesley, Vol. II-15-10.
[17] A. Einstein, Astron. Nachrichten **199**, 7 [1914].
[18] Ref. [10], p. 454.
[19] C. V. Heer, Phys. Rev. **134**, A 799 [1964].